DENTAL MATERIALS 35 (2019) e83–e95

Available online at www.sciencedirect.com

ScienceDirect

journal homepage: www.intl.elsevierhealth.com/journals/dema

Influence of veneer pore defects on fracture behavior of bilayered lithium disilicate glass-ceramic crowns

Yutao Jian[a,1], Li Dao[b,1], Xiaodong Wang[b,1], Xinping Zhang[c], Michael V. Swain[d], Ke Zhao[b,*]

[a] Institute of Stomatological Research, Guangdong Provincial Key Laboratory of Stomatology, Sun Yat-sen University, Guangzhou, China

[b] Department of Prosthodontics, Guanghua School of Stomatology, Sun Yat-sen University; Guangdong Engineering Research Center of Technology and Materials for Oral Reconstruction, Guangdong Provincial Key Laboratory of Stomatology, Guangzhou, China

[c] School of Materials Science and Engineering, South China University of Technology, Guangzhou 510640, China

[d] Dental Materials, Bio-clinical Sciences, Faculty of Dentistry, Kuwait University, Kuwait City, Kuwait

ARTICLE INFO

Article history:
Received 20 June 2018
Received in revised form
28 November 2018
Accepted 13 January 2019

Keywords:
MicroCT
Pore defects
3D characterization
Fracture test
Finite element analysis
Bilayered structure

ABSTRACT

Objective. To identify the conditions under which fabrication pore defects within veneering porcelain in bilayered lithium disilicate glass-ceramic (LDG) crowns will influence and jeopardize the mechanical integrity of the structure.

Methods. Thirty standardized molar crowns (IPS e.max Press) were fabricated and microCT scanned to 3D-analyze the size, morphology and distribution of pores in veneering porcelain, followed by in vitro fracture test and SEM fractographic observation. Finite element analysis (FEA) of the microCT reconstructed models was used to evaluate the stress state.

Results. The volumes of pores in samples ranged from 3241 μm^3 to 1.29×10^9 μm^3 with the equivalent radius between 10 μm to 680 μm. Deviation of sphericity of pores ranged from 0.10 to 0.81 and the average of 99.97% pores was near 0.63. For the smaller pores their distribution tended to be uniform, while the larger pores were irregular with elongated ellipsoidal form and located at or near the veneer–core interface. During wedge loading blunt contact fracture testing 21 crowns failed from the fissure on the occlusal surface, of which 16 failed from surface or near surface pores, 2 from the midpoint of the oblique ridge, and 7 from larger interfacial pores. FEA analysis indicated that defects were detrimental to veneer integrity only in regions of tensile stress and where the pore radius associated with crack initiation ranged from 30 to 50 μm. Pore morphology appeared to have only a minor effect on fracture.

Significance. Within the limitation of the microCT resolution and FEA, it suggests that pores radius large than 30–50 μm and located in the tensile stress area like grooves and fissures on the occlusal surface or near surface as well as cervical margins of veneering porcelain will jeopardize the bilayered structure and mechanical integrity of LDG.

* *Corresponding author at*: Guanghua School of Stomatology, Hospital of Stomatology, Sun Yat-sen University, Guangdong Provincial Key Laboratory of Stomatology, 510055 Guangzhou, China.
E-mail address: zhaoke@mail.sysu.edu.cn (K. Zhao).

[1] Contributed equally to this work.

https://doi.org/10.1016/j.dental.2019.01.016
0109-5641/

1. Introduction

Over the past few decades, dental ceramic materials have been widely used in prosthetic dentistry for their biocompatibility and esthetic outcomes [1]. Esthetic dental ceramics are commonly bilayered systems, with an inner layer of high-strength core ceramic, which is mainly crystalline, and an outer layer of esthetic veneering porcelain primarily a glass matrix [2,3]. However, when veneered with porcelain, bilayered systems had a lower strength and higher failure rate compared to the monolithic system [4]. Delamination and chipping of veneering porcelain were the common outcome in a number of clinically failed bilayered all-ceramic dental restorations [5–8].

Fractographic investigations of clinically failed bilayered ceramic composites showed that pores in veneering porcelain placed the mechanical intergity of bilayered restorations in jeopardy [9,10]. The presence of pores results in stress concentration sites and thus reduces the fracture resistance of all-ceramic restorations [11]. In the literature, the relation of pore defect and the fracture was controversially discussed. Study found that the strength was determined by the size of the largest defect in restorations [12], and pores at the interface or within the veneer layer were not related to adhesive failure or delamination [13]. Yet other studies suggested that the location of pores should be a more important factor leading to the chipping and fracture of restorations [14,15]. It has been also suggested that internal individual pores in veneers appeared to be harmless until they extended to the superficial layer of tensile stressed regions [14,16] or were located at the veneer–core interface [17].

The previous relevant studies were mostly based on the evaluation of pores from 2D sections and might thus distort the shape of pore defects and its relationship to the surroundings, and limit the measured data set due to the complex nature of pore morphology in three-dimensions (3D). Consequently, the authentic causation between pores in bilayered structures and system failure was deemed to be hardly established by the fractographically acquired data. High-resolution microCT and 3D reconstruction provide a nondestructive technique for the study of pores in ceramic materials [18]. In our previous study, both methods have been applied to investigate and characterize the distribution of fabrication defects in bilayered lithium disilicate glass-ceramic (LDG) crowns [19]. We found that LDG strength estimated from pore size was comparable to the values from literature. Large defects were more likely to appear at the core–veneer interface of occlusal fossa, while small defects were also common in every region of the crowns but tended to concentrate in the central fossa region.

Here we present the further study using microCT, followed by finite element analysis (FEA) and in vitro control test, to identify the conditions under which fabrication pore defects within veneering porcelain in clinically common bilayered LDG crowns will essentially influence and jeopardize the mechanical integrity of this bilayered structure.

2. Materials and methods

2.1. Sample preparation and acquisition of the data set

Thirty full-contour LDG molar crowns were fabricated according to manufacturer's instructions. The manufacturing operation of core frameworks (IPS e.max Press, LT A1, Ivoclar Vivadent, Schaan, Liechtenstein) and multi-layering/firing veneering procedure (IPS e.max Ceram, Ivoclar Vivadent, Schaan, Liechtenstein) were performed according to our previous study [19]. Acquisition of the pore defect data-set of LDG was performed using a commercial microCT system (μCT50, SCANCO, Bassersdorf, Switzerland). The protocols used in this study were optimized to visualize the detail of the analyzed defects and were standardized at 90 kV, 155 μA and 14 W with twice averaging of scans, exposure time of 1500 ms, and 0.5 mm aluminium filter. Scanning resolution was set to 2048 × 2048 pixels with 7.4 μm per pixel and 405 μm^3 per voxel size.

The raw data set of each cross-section was converted to *dicom* format and 3D reconstructed using VGStudio max 2.1 (Volume Graphics, Heidelberg, Germany), to provide an axial perspective data of the entire ceramic crown. Pores data were analyzed using module program basing upon threshold segmentation, by which pores were consistent with air and distinguishable from other flaw. Eight voxels were set as the minimum limitation of pores, accordingly, the minimum pore volume should be 3241 μm^3 and 10 μm in radius. Pores inside the veneer were visualized from different perspectives (Fig. 1). Parameters such as size, sphericity, distribution and number were calculated automatically. Sphericity was defined as the morphology of the pore, which is calculated depending on the shapes changing from 0 defined as the pore collapsed to a line, and 1 meaning the pore was a perfect sphere.

After scanning, all crowns were seated and cemented on the resin replicas (P60 Filtek™, 3M ESPE, USA) using adhesive resin (MultilinkN, Ivoclar Vivadent, Liechtenstein). Treatments of the inner and outer surface of crowns plus cementing procedures were performed according to the manufacturer's instruction and a previous study [4]. One hour after cementation, all specimens were stored in distilled water at 37 °C for 24 h prior to testing.

2.2. In vitro experiment

2.2.1. Fracture testing

All crowns underwent single load-to-failure test using a universal testing machine (AG-X 100, Shimadzu, Kyoto, Japan). A 6 mm diameter steel ball (blunt indenter) was placed over the central fissure of the specimen to enable three-point contact according to ISO-6872 [20] and the previous study [21]. A 0.2 mm thick piece of tin foil (Reynolds, USA) was inserted between the loading sphere and specimen to reduce peak stresses at the contact points. Samples were loaded at 0.5 mm/min until delamination and/or cohesive fracture occurred within the veneering porcelain [13]. The fracture loads were recorded in newtons [N] for each specimen and compared with the results of pore analysis in Section 2.1.

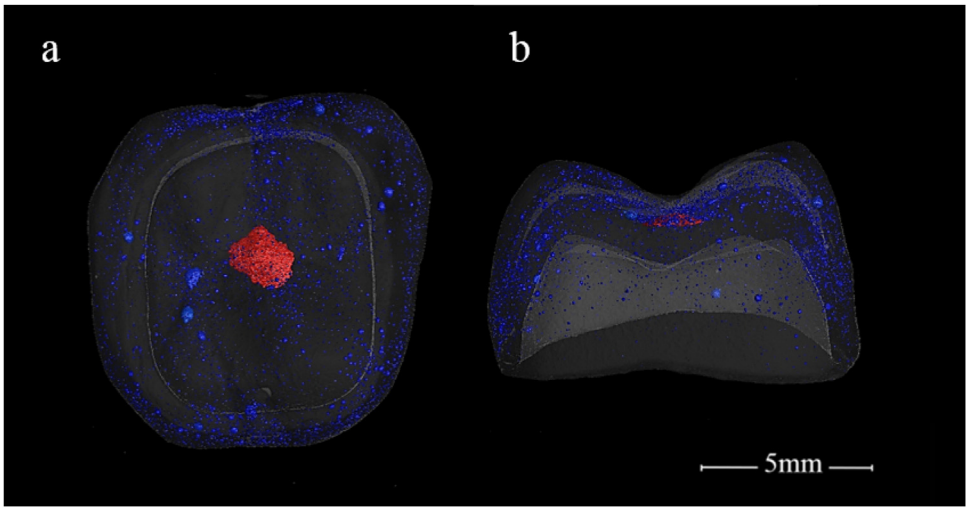

Fig. 1 – Top (a) and lateral (b) views of reconstructed 3D crown from microCT data. Pore defects within the veneer were colored to represent different dimensions.

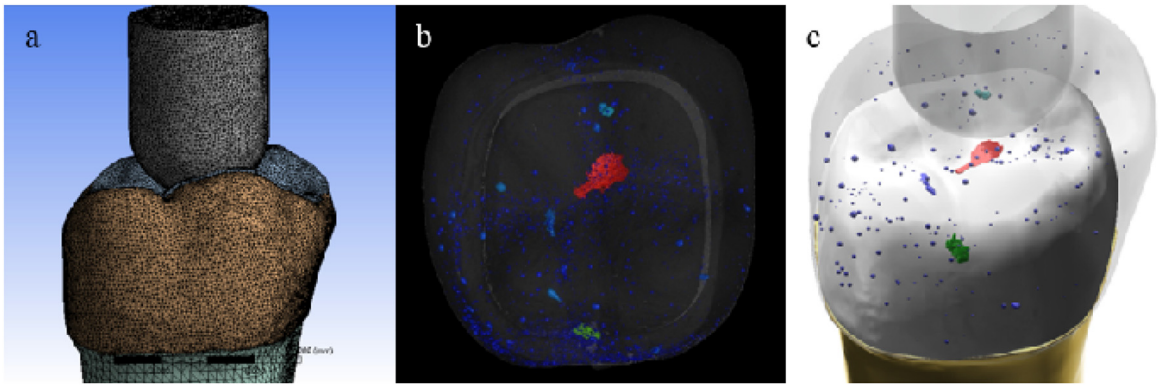

Fig. 2 – (a) FEA model for analog computation, the model was composed of 900,544 elements and 2,255,146 nodes in total with mesh size of 0.2 mm, and the minimum mesh size of pores was set as 0.01 mm in the present study. (b) 3D reconstructed crown and (c) FEA "porous-model", pores were extracted from sample No. 6 and integrated into veneering layer.

Table 1 – Materials properties attributed to the models.

Materials	Young's modulus (GPa)	Poisson's ratio μ
IPS e.max Ceram for veneer	64	0.23
IPS e.max Press for core	95	0.27
Epoxy resin for abutment	17.9	0.31
Blunt indenter	206	0.30
Tin foil	11.8	0.28

2.2.2. *Fractographic morphological observation*

The fractured surfaces of broken crown were observed by scanning electron microscopy (SEM, Quanta 200, FEI, Neatherland) to identify the failure modes and the location, origin and direction of propagation of cracks. Wake hackle markings from the pore defects, cone cracks and radial cracks were selected as references for determination of fracture modes and crack initiation [22].

2.3. *Finite element analysis (FEA)*

Stresses at locations of pores and through the entire crown were simulated using FEA. 3D models constructed directly from microCT results [23]. Each model contained veneering porcelain, core, their abutment, as well as the 0.2 mm tin foil and the blunt indenter. The indenter material was chosen as steel in consistent with the in vitro test. Models were meshed automatically with ANSYS 14.5 (ANSYS, Canonsburg, PA, USA), and composed of 900,544 elements and 2,255,146 nodes in total with mesh size of 0.2 mm for analog computation. The minimum mesh size of pores was set in 0.01 mm since the smallest pore radius was 0.01 mm in the present study (Fig. 2a). An ideal model without pore defects was set up to compare the fabricated crown with pores in reality. The presence of "real" pores in a "porous model" were extracted from one of the fabricated samples as reference, and integrated into the

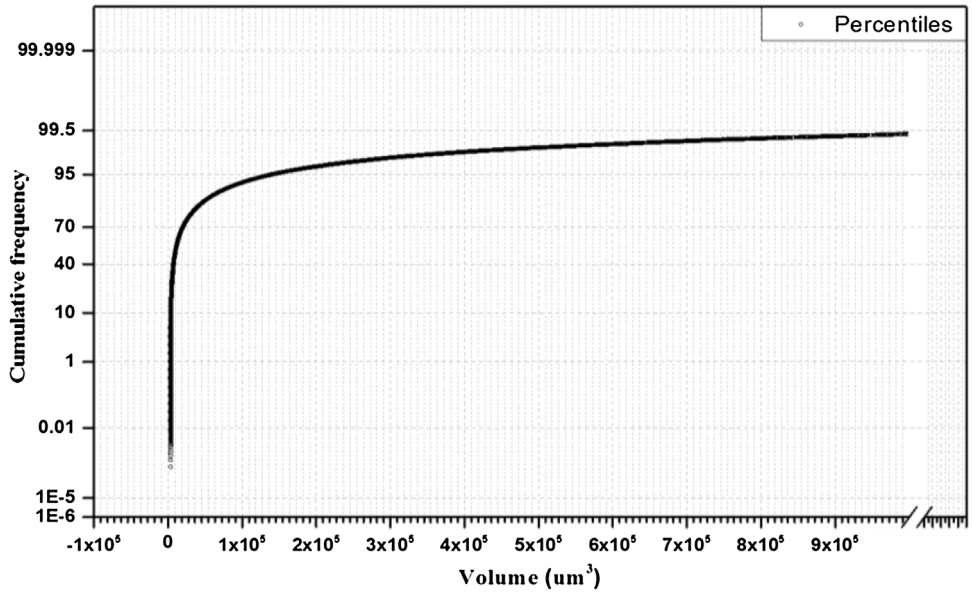

Fig. 3 – Kaplan–Meier's cumulative frequency of pore volumes in all samples.

Table 2 – Relative frequency of each pore volume range.

Range	Volume range (μm^3)		Equivalent radius (μm)		Relative frequency
1	3.241 to	10^5	10	29	92.72%
2	10^5 to	10^6	29	63	6.67%
3	10^6 to	10^7	63	135	0.58%
4	10^7 to	10^9	135	680	0.03%

veneering porcelain layer (Fig. 2b and c). The general effect of pores on the stress concentration was investigated based upon the results from the pores analysis in Section 2.1, and detail information is listed in Section 3.3.2. The values of the material properties used in the FEA analysis are listed in Table 1 [23–26].

A downward displacement of 0.6 mm was applied to the blunt indenter to simulate in vitro loading. Based upon the feasible computing time cost and calculating ability of the whole system, the value of displacement we used was set according to the average displacement of indenter from initial contact to fracture. As it is a linear elastic analysis, the choice of displacement and associated load does not affect patterns and distribution of stress in the model. The bottom surface of the abutment mesh was fixed in all three spatial dimensions and was the boundary condition. Interfaces between veneer, core and abutment were considered perfectly bonded, and the material was considered isotropic and homogeneous [23,27]. As the condition for the onset of fracture was required the maximum principal stress distribution was emphasized [28].

2.4. *Statistical analysis*

The possible relationship of fracture load, max pore volume and pore number were analyzed with Pearson's correlation using SPSS 15.0 (IBM, Armonk, US). Parameters were considered statistically significant at the level of 0.05.

3. Results

3.1. *Pore defects*

3.1.1. *Size*

The distribution of pore volumes in all samples ranged from 3241 μm^3 to 1.29×10^9 μm^3, and the equivalent radius was between about 10 μm to 680 μm. 99% of pore volumes was less than 1,000,000 μm^3 or 63 μm in equivalent radius (Fig. 3). Depending upon volume, pores were divided into four ranges, 3.241–10^5 μm^3, 10^5–10^6 μm^3, 10^6–10^7 μm^3 and >10^7 μm^3 (Table 2).

3.1.2. *Morphology*

Cumulative frequency of sphericity (a) in the different volume ranges (b), are shown in Fig. 4. Sphericity of pores ranged from 0.10 to 0.81 (Fig. 4c). In general, 96.5% of the pores were more than 0.5. The lower sphericity of pores suggests the more complexity in shape. The average sphericity of each range was 0.62, 0.62, 0.64 and 0.42, respectively, i.e. the sphericity of 99.97% pores (Section 1–3) was near 0.62–0.64, and had a comparable trend.

3.1.3. *Distribution in veneer*

The veneering porcelain contained pore defects of different sizes. With the decrease of the pore size, the distribution tended to be uniform in the different crowns. Pores with vol-

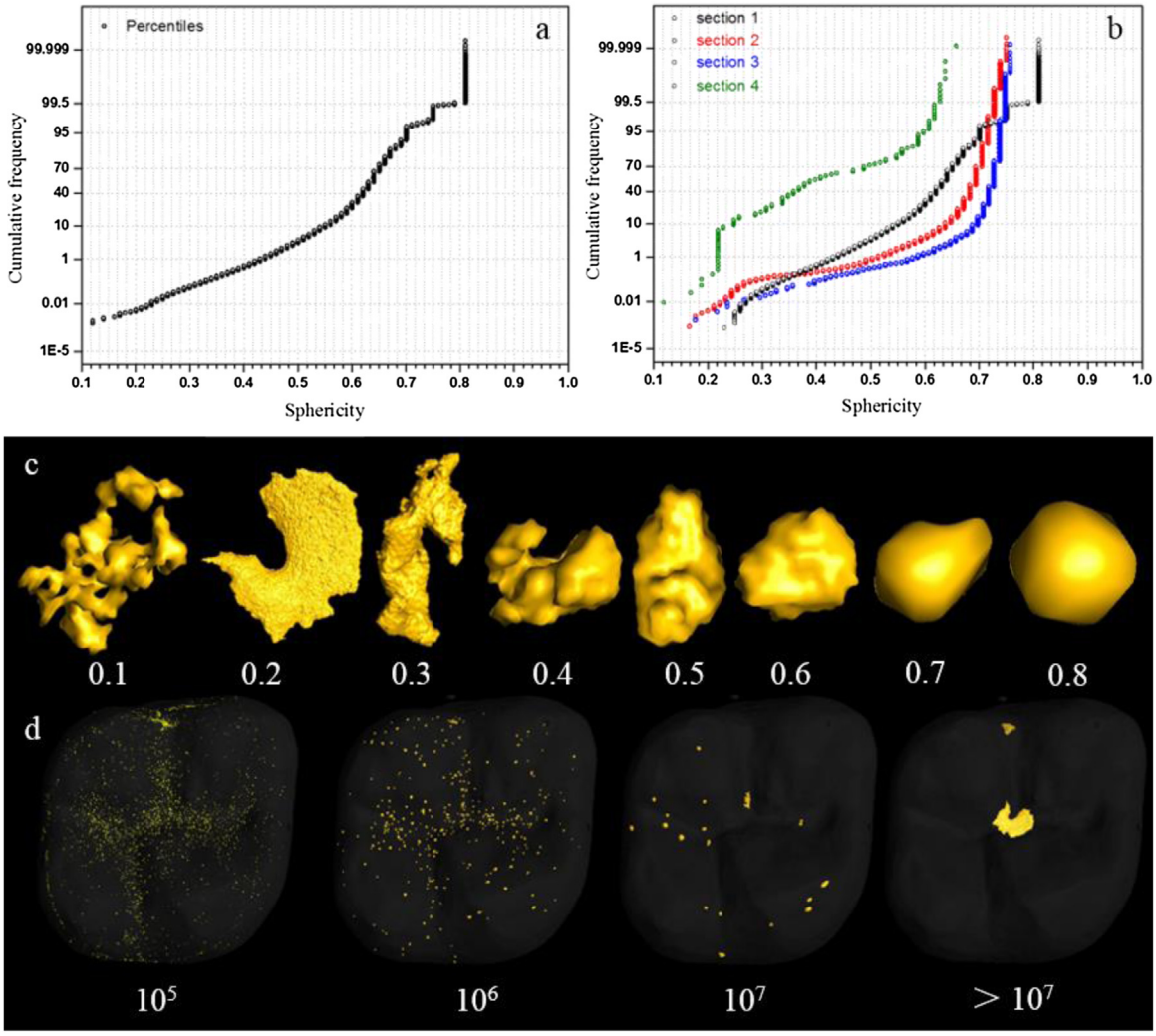

Fig. 4 – (a) The cumulative frequency of sphericity for all pores, and (b) in the different volume ranges. (c) Examples of pores 3D morphology with different degrees of sphericity. (d) The typical distribution of the different ranges of pores in crowns.

ume under 10^6 μm^3 were located covering the cusps, central fossa, occlusal fossa, axial wall and margins (Fig. 4d).

The bulky or larger pores were irregular, with an elongated ellipsoidal form and located at or near the veneer–core interface (Table 3).

Based upon the above results, a general pattern of pores within veneering porcelain is drawn schematically (Fig. 5). Pores were everywhere in the veneer with most of these pores being small (<63 μm) and near spherical in shape (>0.6). Almost every sample contained isolated large, irregular bulky pores along the veneer–core interface, especially in the region of central or occlusal fossa. The long axis of the bulky pores trends to parallel with the tangent plane at the contact point of interface. Neither of the large defects was found to align perpendicular to the interface.

3.2. *In vitro experiment*

All crowns showed bulk fracture with cracks propagating in the mesio-distal plane and separating the crown into two pieces. The mean fracture load ($x \pm sd$) was 1951.7 ± 361.1 N.

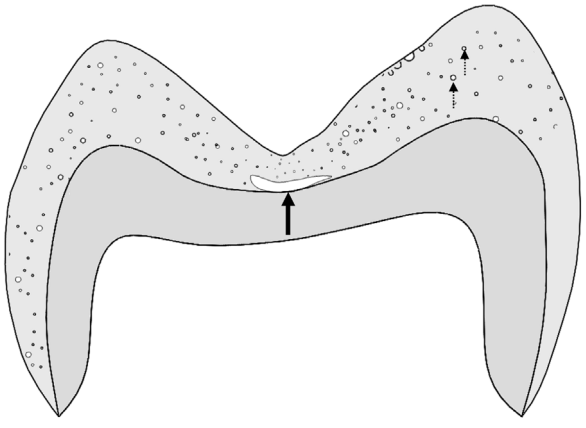

Fig. 5 – Schematic sketch of the general pattern of pore defects within veneering porcelain. Black solid arrows represented the large and irregular bulky pores at or near the interface, whilst black dashed arrows indicate the major small spherical-shaped pores.

Table 3 – Pore parameters and fracture findings of each crown.

Sample	Numbers	Max volume (μm^3)	Max location[a]	Fracture load (N)	Fracture origin	Fracture origin crack size (μm)
1	14,381	2.53×10^8	OF-AW	1318	Occlusal surface, occlusal fissure defects	50
2	9128	2.58×10^8	CF	1396	Occlusal surface, occlusal fissure defects	35
3	43,154	5.41×10^8	CF	1420	Core–veneer interfacial defects	5.41×10^8
4	16,180	4.21×10^7	AW	1434	Occlusal surface, occlusal fissure defects	35
5	28,965	8.93×10^7	OF	1521	Occlusal surface, occlusal fissure defects	35
6	12,658	1.58×10^8	CF	1550	Occlusal surface, occlusal fissure defects	1.58×10^8
7	13,256	1.09×10^8	OF	1555	Occlusal surface, occlusal fissure defects	42
8	9847	3.82×10^7	CF	1660	Occlusal surface, occlusal fissure defects	200
9	19,541	8.73×10^8	CF	1661	Occlusal surface, occlusal fissure defects	50
10	13,245	1.52×10^6	OF	1700	Occlusal surface, occlusal fissure defects	40
11	8146	1.87×10^8	OF-AW	1762	Occlusal surface, occlusal fissure defects	30
12	6587	2.35×10^7	CF	1841	Blunt contact	Null
13	9512	1.29×10^7	OF	1853	Occlusal surface, occlusal fissure defects	48
14	7548	8.95×10^6	OF	1854	Occlusal surface, occlusal fissure defects	180
15	8529	1.68×10^7	CF	1889	Occlusal surface, occlusal fissure defects	Null
16	8358	2.60×10^8	OF	1895	Blunt contact	Null
17	7295	4.21×10^7	CF	1962	Core–veneer interfacial defects	4.21×10^7
18	24,521	2.73×10^7	CF	2017	Occlusal surface, occlusal fissure defects	80
19	8451	1.25×10^7	CF	2061	Occlusal surface, occlusal fissure	Null
20	11,584	2.54×10^7	OF	2077	Occlusal surface, occlusal fissure defects	45
21	7995	6.88×10^7	CF	2080	Core–veneer interfacial defects	6.88×10^7
22	19,257	6.75×10^6	CF	2095	Core–veneer interfacial defects	1.28×10^6
23	7254	4.25×10^7	OF-AW	2334	Occlusal surface, occlusal fissure	Null
24	9794	5.19×10^7	CF	2460	Occlusal surface, occlusal fissure defects	60
25	32,145	8.27×10^7	CF	2514	Occlusal surface, occlusal fissure	Null
26	18,173	3.48×10^8	OF	2574	Occlusal surface, occlusal fissure	Null
27	12,626	4.96×10^8	CF	2618	Occlusal surface, occlusal fissure	Null
28	6752	5.25×10^7	AW	2660	Core–veneer interfacial defects	1.25×10^7
29	14,229	4.27×10^8	OF	2685	Core–veneer interfacial defects	4.27×10^8
30	10,589	3.68×10^7	CF	2884	Core–veneer interfacial defects	2.31×10^6

[a] OF = occlusal fossa, CF = central fossa, AW = axial wall.

Table 4 – Individual pore model attributed to the FEA.

Pores	Volume (μm^3)	Sphericity
1	3241	0.6
2	10^5	0.6
3	10^6	0.6
4	4	0.6
5	5.21×10^8	0.2

The SEM observations of samples and the results of VGStudio showed different fracture origins in the crowns and the size of the crack defect (Table 3). No correlation between the fracture load and the situation of pores was found ($p > 0.05$).

21 crowns failed from the fissure on the occlusal surface. Critical cracks originated from the base of the fissure and grew deeply into the veneering ceramic forming semi-circular crack patterns that intersected with and extended through the supporting ceramic core. Among the 21 crowns, 16 failed from surface or near surface pores and 5 from surface of veneer (Fig. 6a). 3D reconstruction of a fractured crown showed that no large or distorted pores were related to the surface fracture, and the fracture does not originate from the interfacial largest pore, even if it was a sharp (planar-like) void (Fig. 6b).

In 2 of the 30 sample, fracture initiated from the midpoint of the oblique ridge, almost directly under the contact point of the blunt ball wedge loading. The crack extended and penetrated deeply along the mesio-distal direction, eventually resulting in bulk fracture. Structural bulky voids were found in the vicinity of the core–veneer interface but seemed to be irrelevant to sample failure. A small pore was observed in the contact region (Fig. 6c and d).

Fracture of 7 specimens initiated from the interfacial largest bulky pore defect, which lay directly below the corresponding contact region (Fig. 6e and f).

3.3. FEA

3.3.1. *Stress distribution in vitro test*

FEA analysis of the contact loading indicated two stress concentration areas were formed, tensile stresses area (Region 1) and high compressive stresses in the blunt contact area but underlying tensile stresses at the veneer–core boundary (Region 2) (Fig. 7). Region 1 was the maximum tensile stress concentrated area, in which tensile stresses occurred mainly at the occlusal fissures — especially at the mesio-distal fissure of the veneer surface. Region 2, tensile stresses concentrated at the intaglio (cementation) surface of the core, as well as the veneer–core interface, in the area directly opposed to the load site and in the external surface of the veneer, near to the loading area.

3.3.2. *Mechanical effects of pores in stress concentrated areas*

For models with pores, the maximum tensile stress values were raised only at the pores located in tensile stress areas. No tensile stress was concentrated at any other pores (Fig. 8).

Five individual pores were constructed based upon the results of Section 3.1 (Table 4). Pore ranges from 1 to 4 represented the general, ubiquitous pores in the veneer while pore size 5 were those associated with the bulky voids at the interface. Pores were subsequently considered only in the two tensile stress areas, Region 1 and Region 2, respectively. Pore sizes 1–4 were placed in the regions of near surface (NS), internal (IN) and the interface (IF), simulating different depths in veneer (Fig. 9a), whilst pore size 5 was considered only at the interface.

In Region 1, pores gave rise to stress concentration only when located near the surface, where localized tensile stress increased. The maximum principal stresses rose with increased pore volume. No stress concentration was observed for pores lying in the other 2 areas. Whilst pores resulted in stress concentration in the contact region, the maximum principal stress was more dependent on its location rather than to pore size. With the location of the pore deeper in the veneer, the maximum principal stresses declined. High stress concentrated at the near surface area, especially where it approached the indenter contact area, and less stress concentration was found at the core–veneer interface. Little or no stress concentrated at the interfacial bulky pore defects in both regions (Fig. 9b, c and f). All 26 models have been constructed in both regions, with 13 each.

4. Discussion

Pore defects in the veneer of bilayered ceramic occurred in each clinical crown examined suggesting that pore formation is an inevitable outcome of the manual layering procedure and sintering process. To identify the conditions under which fabrication pores defects will essentially influence and jeopardize the bilayered structure mechanical integrity potentially sheds light on the subsequent quality control procedures in the clinic.

In the present study, pores were observed in every part of the veneering porcelain. The morphology of most pore defects was small and homogeneous while a few were bulky. These defects form during the layering and sintering process of fabrication [29,30]. In general, pores formed in such a way are small, regular and homogenously distributed. In our results, 99% of pores presented such common characteristics. In practice, crowns with such types of pore defects are not rejected from clinical use. Thus, the question rises as to where are the pores related to the clinical failure of the crown originates located?

Pore defects occur due to porcelain sintering shrinkage in the range of 13%–17% [31]. If bubbles or vacancies are present prior to sintering then at the shrinking center, the space will be stretched during the sintering, resulting in a large void. Most of crowns contained such large and bulky pores in this study and the bulky pores trended to lie parallel to the interface. In literature, these pore defects related to crown failure can be largely, if not entirely, attributable to such bulky pores whose size exceeds a certain dimension or are at a critical location [16].

From the in vitro contact loading tests conducted we found that two types of pores resulted in fracture: surface or near surface pores, and interfacial bulky pores, which is in accordance with previous results [15,16,17,32]. FEA showed that as the compressive force loaded onto the cusp bevels, tensile stress became raised both at the occlusal fissures and at the interface

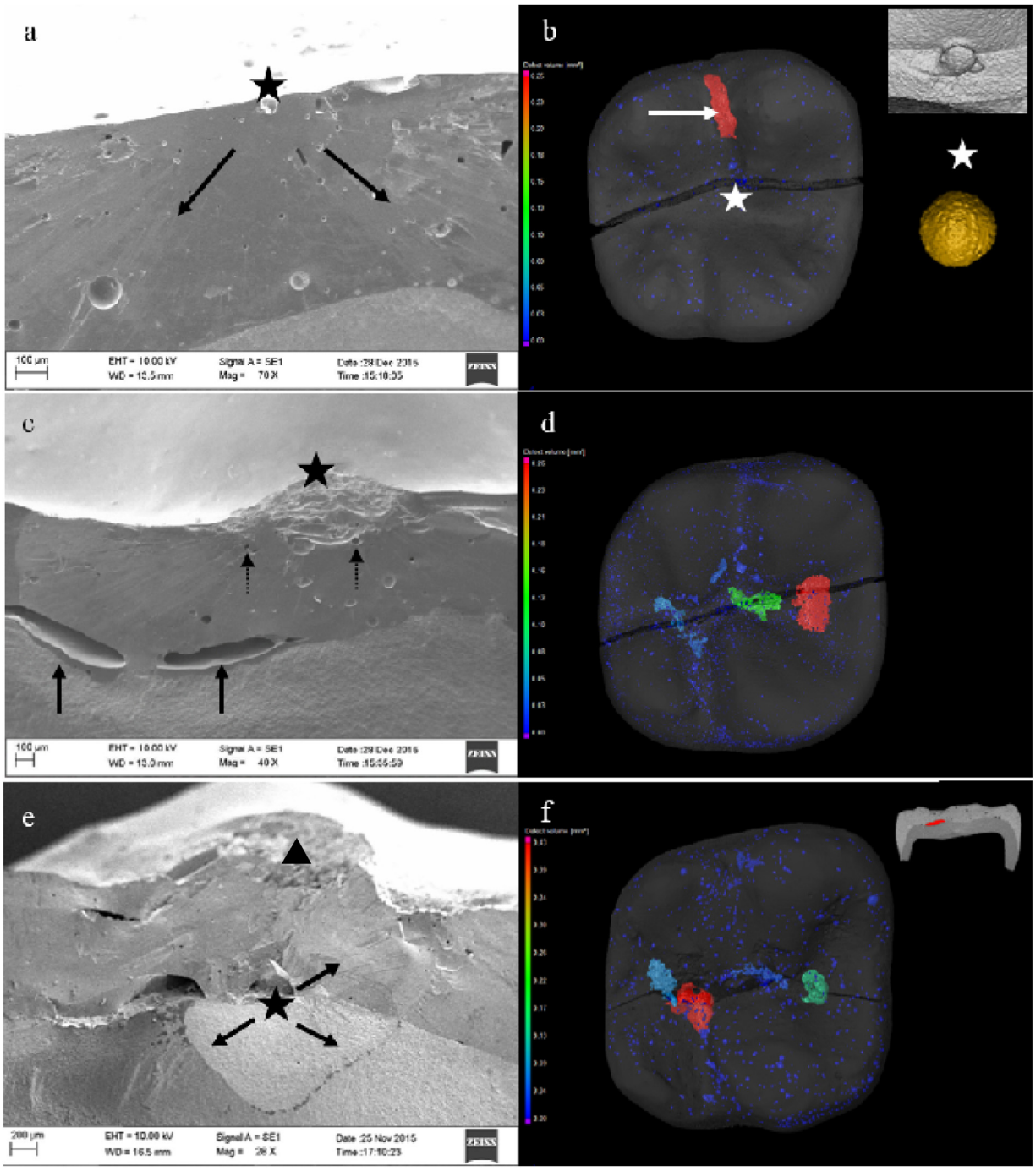

Fig. 6 – (a) Shows a failed crown with crack initiation from a surface pore. The black star indicates the fracture origin, while the black solid arrows indicate the direction of crack propagation (SEM, 70×). (b) 3D reconstruction of the pores responsible for the surface fracture. In this image the white stars indicate the fracture origin, and white arrows an interfacial bulky pore. (c) and (d) are SEM and 3D reconstruction images of a failed specimen. Black solid arrows indicate the bulky interface pore (SEM, 40×), while black dashed arrows indicate small pores in the contact region. (e) In this image the crack initiates from a bulky interfacial pore defect. The black triangle is the blunt contact region (SEM, 20×). (f) 3D reconstruction of the large and sharp planar like-pores responsible for interfacial fracture.

below the contact region. The stress was found to concentrate at the pores, especially if the pores were located in the tensile stress areas: in the first main tensile stress zone like occlusal fissure, the tensile stress would reach a peak drastically as long as the pore radius was, independent of its morphology, larger than 30 μm; in the second tensile stress zone like core–veneer interfacial as well, such bulky pore was also able to lead to high tensile stress concentration. This relationship of position and dimension of pore defect to its stress situation was deemed to nevertheless not occur outside of the stress concentration

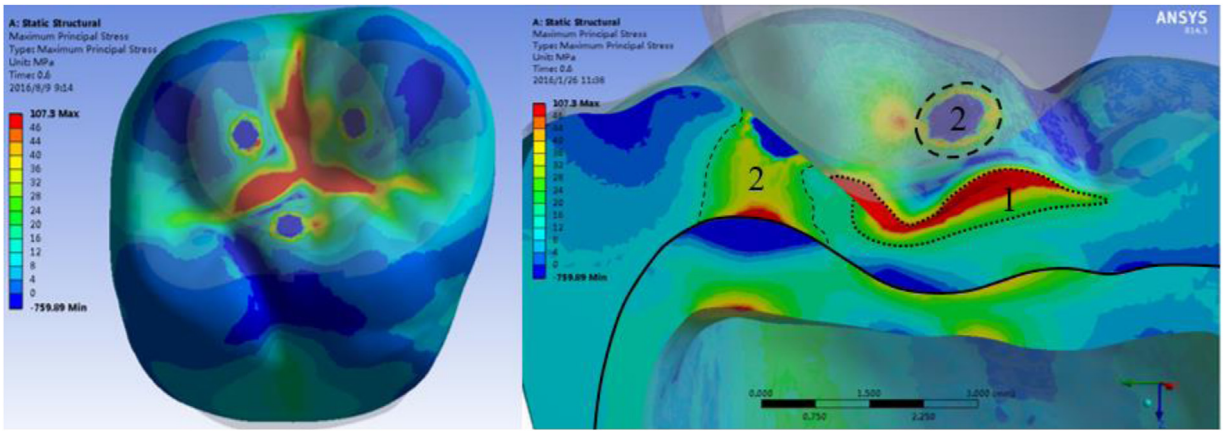

Fig. 7 – Blunt contact loading induced stress distribution in the veneer. Region 1 and Region 2 are the two main stress concentration areas.

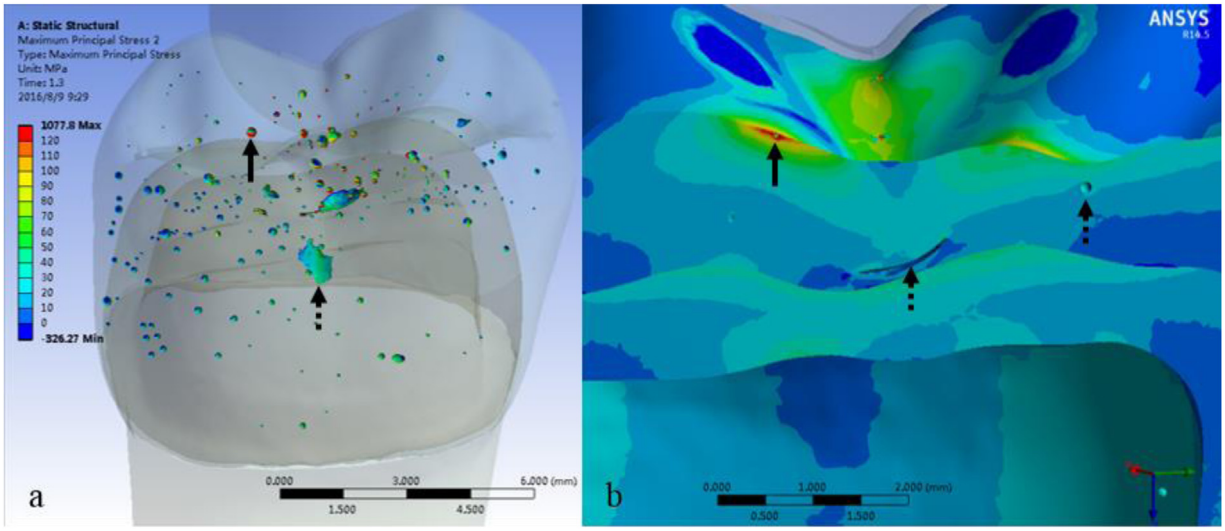

Fig. 8 – (a) Stress distribution in the model with pores. (b) Tensile stress only concentrates at the pores located in Region 1 and Region 2. Black solid arrows indicate the stress concentration of pore, and black dashed arrow indicates pores without high stress even though they were large and distorted.

areas. Our data clearly demonstrated that pore defects, when their dimension reached a certain value, were detrimental to veneer integrity only when located in the tensile stress area, whereas in unstressed areas pores appeared to be harmless even though they were large and distorted. Our finding was consistent with previous research, which suggest that pores in glass are not initially viewed as flaws but rather as blunt stress concentration sites [14]. Also it is well known that veneering porcelain contains a high quantity of glass matrix [33].

Based upon the FEA simulation, we found that pores close to the indenter contact area showed high tensile stress concentration, whilst the maximum principal stress attenuated with the pore located deeper into the veneer. The contact associated with the fracture test, also known as blunt contact, simulated an important form of loading in many dental ceramic-based structures [34]. Two competing damage modes were identified when blunt contact occurred in the ceramic: cone cracking and quasi-plasticity [35]. The contact zone as well as the high-localized Hertz stresses formed during loading often resulted in a ring shaped crack encircling this area. The pore defects would therefore lead to high stress concentration around themselves when the pores were adjacent to the contact region. In comparison, the quasi-plasticity damage mode would not occur beneath the contacts since the veneering porcelain is a glass matrix based brittle material and had no visible subsurface quasi-plasticity damage [35]. Pore defects lying beneath the contact regions would be able to withstand the stress prior to fissure induced cracking. Our results, upon combining the in vitro test and FEA, suggested that pore defects close to the indenter contact area were deemed relevant to fracture, whereas internal pores away from the contact area appeared to be less harmful.

Since the maximum principal stress attenuated with the pore located deeper into the veneer, the pore defects lying at the interface to core must have suffered much less stress in comparison with those at or near surface. Such pore defects

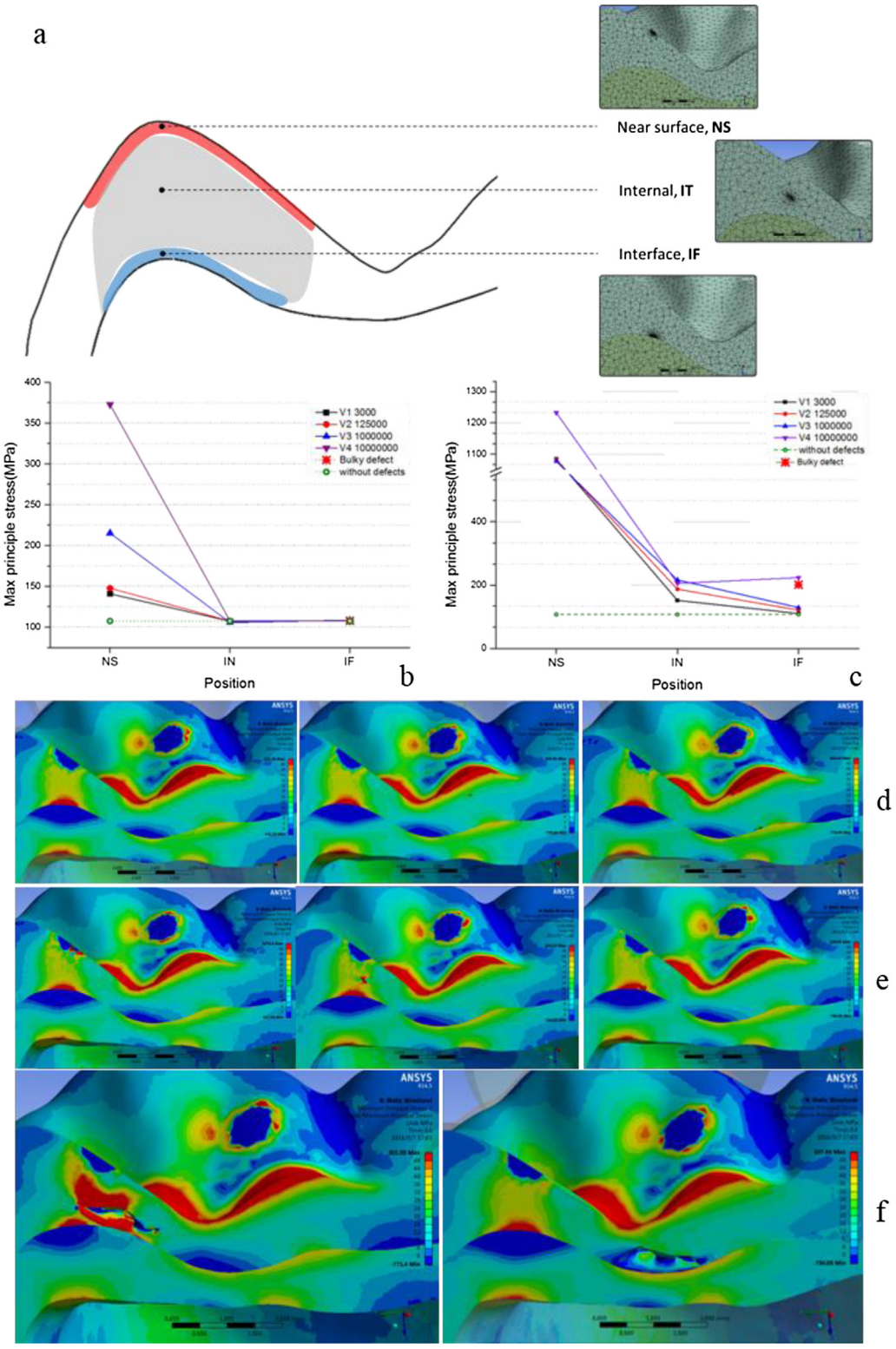

Fig. 9 – (a) Different positions of pore defect; (b)(d) Pore stress in tensile stress concentrated area (Region 1); (c)(e) Pore stress in load contact area (Region 2); (f) The distinguishable mechanical effects of bulky pore at interface of Region 2 as well as Region 1.

lying at the interface have been researched [17,36]. In the present study, 3 crown samples fractured from bulky pores at the interface. We assessed the failure strength of pores at the interface via the fracture energies leading to fracture according to the relationship of strengths and pore size [14],

$$\sigma = Z\sqrt{\frac{E\gamma}{a}} \quad (1)$$

where σ is the failure tensile strength, E Young's modulus, γ the fracture surface energy, a the flaw size and Z is a parameter set as 1.25. Though failure strength is not capable of being calculated directly when the pore morphology is irregular, it can be replaced by the failure load N and estimated approximately. So a relation of $\gamma \propto a\,N^2$ can be derived. Accordingly, the average fracture load N (2241 N) causing fracture of pore defects at the interface was higher than that (1711 N) for the pore at surface or near surface. Thus, the interfacial pore defects required more energy, and further, more load onto themselves, till fractured than those at or near surface ones. It clearly suggested that these pores at the interface withstood the stress tougher than those at or near surface on one hand, while they suffered from less stress, with other words, less load burthen in those tensile environments on the other hand. Taken together, the interfacial pore defects would less likely cause fracture in comparison.

In the present in vitro fracture test indeed, 16 of 30 crown samples contained interfacial bulky pores, not all of them nevertheless caused fracture, only 3 fracture samples were found to be linked to the interfacial pore defects. In contrast, pores in 7 fracture samples located directly under the contact zone and caused stress concentration. In comparison, results from zirconia or alumina bilayered porcelain veneered structures show that interfacial flaws are important for crack initiation [37,38]. The difference between LDG and zirconia/alumina core materials with respect to the stress resistance of veneering porcelain with pore defects appeared to be attributable to other factors. In particular the elastic modulus of the veneer material matches closely with the LDG and both materials bond well at the interface as they infiltrate into each well [27]. In addition, the large mismatch in elastic moduli and fracture toughness between the veneering material and zirconia/alumina often make it difficult for the crack to cross the interface causing chipping delamination rather than complete veneer and core fracture to occur [39–41]. Based upon the present FEA analysis, we assumed that residual stresses resulting from thermal expansion mismatch between the core and veneering material, and residual tempering stresses associated with the cooling procedure during the final stage of preparation of bilayered LDG, were not significant in terms of stresses developed. It must be an interesting new topic whether such residual stresses determine the fracture strength of veneered LDG and how such stresses might change the ease at which the pores as encountered in this study may contribute to failure.

In clinic, single point contact on the occlusal area like biting something hard is common. In the present result, the tensile stresses became highly concentrated at the central fossa and surrounding cusp as well as cervical margin. A recent study has shown that grooves, fissures as well as cervical margins on the occlusal surface are critical locations where tensile stresses concentrate regarding to chewing [42]. Since pore defects appeared to be detrimental in the tensile stress area in bilayered LDG crowns, it suggested that pores located at grooves, fissures as well as cervical margins on the occlusal surface or near surface of veneering porcelain would influence and potentially jeopardize the mechanical integrity of bilayered LDG structure.

Once the type and location of potentially detrimental pore defects have been identified, the question arises as to which pore size seems most likely for being responsible for crack initiation in tensile stress areas. When a pore defect is the critical flaw and eventually leads to the fracture of veneering porcelain, the pore radius will conform to the following relation of strength to fracture toughness [12],

$$\sigma = \frac{K_{ic}}{1.25\sqrt{\pi c}} \quad (2)$$

where K_{ic} is the fracture toughness and c the radius of the pore defect [43]. The fracture toughness and strength of IPS e.max Ceram are reported to be 0.7 MPa $m^{1/2}$ [33] and 90 ± 10 MPa, resulting in critical pore radius c of 30 μm–50 μm respectively. The value was very close to the pore size of flaws at the fracture origin in tensile area in the present study (FEA and in vitro experiment), and a previous study as well [32]. Upon combining the analysis of all the micro-CT results, about 7% of the pores in the veneer were larger than this threshold.

In the present study, we used FEA to simulate the in vitro fracture loading test, but the limit of transferring lab to virtual results should be taken into consideration [23,44]. In general, models of ceramic crown are simplified by FEA under which: (i) materials are considered homogeneous, isotropic and the elastic behavior represents itself linear; and (ii) residual stresses induced by thermal mismatch of the materials are not included. The 3D FEA in such a way was deemed to be, though powerful, not capable of rebuilding all the conditions from reality. And the real influence of the cement layer as well as the bonding state and friction coefficient between different layers were hard to be simulated.

5. Conclusions

Within the limitation of the microCT resolution and FEA, it suggests that pores radius large than 30 μm–50 μm and located in the tensile stress area like grooves and fissures on the occlusal surface or near surface as well as cervical margins of veneering porcelain may potentially influence and jeopardize the mechanical integrity of bilayered LDG structures.

Acknowledgments

This work was supported by the National Natural Science Foundation of China under grant No. 81470767, 81771110 and 81600907.

REFERENCES

[1] Lawson NC, Burgess JO. Dental ceramics: a current review. Compend Contin Educ Dent 2014;35:161–8.

[2] Nakamura K, Harada A, Inagaki R, Kanno T, Niwano Y, Milleding P, et al. Fracture resistance of monolithic zirconia molar crowns with reduced thickness. Acta Odontol Scand 2015;73:1–7, http://dx.doi.org/10.3109/00016357.2015.1007479.

[3] Pavlović VB, Vulićević Z, Pavlović VP. Contemporary dental ceramics. Proceedings of the IV Advanced Ceramics and Applications Conference 2017. Atlantis Press.

[4] Zhao K, Pan Y, Guess PC, Zhang XP, Swain MV. Influence of veneer application on fracture behavior of lithium-disilicate-based ceramic crowns. Dent Mater 2012;28:653–60, http://dx.doi.org/10.1016/j.dental.2012.02.011.

[5] Simeone P, Gracis S. Eleven-year retrospective survival study of 275 veneered lithium disilicate single crowns. Int J Periodontics Restor Dent 2015;35:685–94, http://dx.doi.org/10.11607/prd.2150.

[6] Makarouna M, Ullmann K, Lazarek K, Boening KW. Six-year clinical performance of lithium disilicate fixed partial dentures. Int J Prosthodont 2011;24:204–6.

[7] Sailer I, Gottnerb J, Kanelb S, Hammerle CH. Randomized controlled clinical trial of zirconia-ceramic and metal-ceramic posterior fixed dental prostheses: a 3-year follow-up. Int J Prosthodont 2009;22:553–60.

[8] Conejo J, Nueesch R, Vonderheide M, Blatz BM. Clinical Performance of All-Ceramic Dental Restorations. Curr Oral Health Rep 2017;4:1–12, http://dx.doi.org/10.1007/s40496-017-0132-4.

[9] Quinn J, Quinn G, Kelly J, Scherrer S. Fractographic analyses of three ceramic whole crown restoration failures. Dent Mater 2005;21:920–9, http://dx.doi.org/10.1016/j.dental.2005.01.006.

[10] Taskonak B, Mecholsky Jr, Anusavice KJ. Fracture surface analysis of clinically failed fixed partial dentures. J Dent Res 2006;85:277–81, http://dx.doi.org/10.1177/154405910608500314.

[11] Abu-Hassan MI, Abu-Hammad OA, Harrison A. Strains and tensile stress distribution in loaded disc-shaped ceramic specimens: an FEA study. J Oral Rehabil 1998;25:490–5, http://dx.doi.org/10.1046/j.1365-2842.1998.00267.x.

[12] Danzer R, Lube T, Supancic P. Fracture of ceramics. Adv Eng Mater 2008;10:275–98, http://dx.doi.org/10.1002/9783527631735.ch12.

[13] Zhao K, Wei Y, Pan Y, Zhang XP, Swian MV, Guess PC. Influence of veneer and cyclic loading on failure behavior of lithium disilicate glass-ceramic molar crowns. Dent Mater 2014;30:164–71, http://dx.doi.org/10.1016/j.dental.2013.11.001.

[14] Rice RW. Pores as fracture origins in ceramics. J Mater Sci 1984;19:895–914, http://dx.doi.org/10.1007/bf00540460.

[15] Kelly JR, Tesk JA, Sorensen JA. Failure of all-ceramic fixed partial dentures in vitro and in vivo: analysis and modeling. J Dent Res 1995;74:1253–8, http://dx.doi.org/10.1177/00220345950740060301.

[16] Quinn GD, Hoffman K, Quinn JB. Strength and fracture origins of a feldspathic porcelain. Dent Mater 2012;28:502–11, http://dx.doi.org/10.1016/j.dental.2011.12.005.

[17] Thompson JY, Anusavice KJ, Naman A, Morris HF. Fracture surface characterization of clinically failed all-ceramic crowns. J Dent Res 1994;73:1824–32, http://dx.doi.org/10.1177/00220345940730120601.

[18] Caty O, Buffiere J, Maire E, Adrien J. 3D characterization of the influence of porosity on fatigue properties of a cast Al alloy. Adv Eng Mater 2011;13:194–8, http://dx.doi.org/10.1002/adem.201000236.

[19] Jian YT, He ZH, Dao L, Swian MV, Zhao K. Three-dimensional characterization and distribution of fabrication defects in bilayered lithium disilicate glass-ceramic molar crowns. Dental Mater 2017;33:e178–85, http://dx.doi.org/10.1016/j.dental.2017.01.009.

[20] ISO-6872: dentistry-ceramic materials; 2015 https://www.iso.org/standard/59936.html.

[21] Albrechta T, Kirstenb A, Kapperta HF, Fischerb H. Fracture load of different crown systems on zirconia implant abutments. Dent Mater 2011;27:298–303, http://dx.doi.org/10.1016/j.dental.2010.11.005.

[22] Scherrer SS, Quinn GD, Quinn JB. Fractographic failure analysis of a Procera® AllCeram crown using stereo and scanning electron microscopy. Dent Mater 2008;24:1107–13, http://dx.doi.org/10.1016/j.dental.2008.01.002.

[23] Della Bona Á, Borba M, Benetti P, Duan YY, Griggs JA. Three-dimensional finite element modelling of all-ceramic restorations based on micro-CT. J Dent 2013;41:412–9, http://dx.doi.org/10.1016/j.jdent.2013.02.014.

[24] Isgró G, Addison O, Fleming GJP. The deformation and strength of a dental ceramic following resin-cement coating. J Dent 2011;39:122–7, http://dx.doi.org/10.1016/j.jdent.2010.10.015.

[25] Isgró G, Addison O, Fleming GJP. Transient and residual stresses induced during the sintering of two dentin ceramics. Dent Mater 2011;27:379–85, http://dx.doi.org/10.1016/j.dental.2010.11.018.

[26] Albakry M, Guazzato M, Swain MV. Biaxial flexural strength, elastic moduli, and x-ray diffraction characterization of three pressable all-ceramic materials. J Prosthet Dent 2003;89:374–80, http://dx.doi.org/10.1067/mpr.2003.42.

[27] Wang XD, Jian YT, Guess PC, Swain MV, Zhang XP, Zhao K. Effect of core ceramic grinding on fracture behaviour of bilayered lithium disilicate glass-ceramic under two loading schemes. J Dent 2014;42:1436–45, http://dx.doi.org/10.1016/j.jdent.2014.03.014.

[28] Thompson MC, Field CJ, Swain MV. The all-ceramic, inlay supported fixed partial denture. Part 2. Fixed partial denture design: a finite element analysis. Aust Dent J 2011;56:302–11, http://dx.doi.org/10.1111/j.1834-7819.2011.01341.x.

[29] Fleming G, Shelton RM, Marquis PM. The influence of clinically induced variability on the bi-axial fracture strength of aluminous core porcelain discs. Dent Mater 1999;15:62–70, http://dx.doi.org/10.1016/s0300-5712(99)00036-6.

[30] Wang AJ, Zhang J, Li JM, Ma AB, Liu LT. Effect of liquid-to-solid ratios on the properties of magnesium phosphate chemically bonded ceramics. Mater Sci Eng C Mater Biol Appl 2013;33:2508–12, http://dx.doi.org/10.1016/j.msec.2013.02.014.

[31] Rasmussen ST, Ngaji-Okumu W, Boenke K, Brien WJ. Optimum particle size distribution for reduced sintering shrinkage of a dental porcelain. Dent Mater 1997;13:43–50, http://dx.doi.org/10.1016/s0109-5641(97)80007-3.

[32] Lohbauer U, Amberger G, Quinn GD, Scherrer SS. Fractographic analysis of a dental zirconia framework: a case study on design issues. J Mech Behav Biomed Mater 2010;3:623–9, http://dx.doi.org/10.1016/j.jmbbm.2010.07.004.

[33] Tang X, Nakamura T, Usami H, Wakabayashi K, Yatani H. Effects of multiple firings on the mechanical properties and microstructure of veneering ceramics for zirconia frameworks. J Dent 2012;40:372–80, http://dx.doi.org/10.1016/j.jdent.2012.01.014.

[34] Jung YG, Wuttiphan S, Peterson IM, Lawn BR. Damage modes in dental layer structures. J Dent Res 1999;78:887–97, http://dx.doi.org/10.1177/00220345990780040901.

[35] Petersonl IM, Pajares A, Lawn BR, Thompson VP, Rekow ED. Mechanical characterization of dental ceramics by Hertzian contacts. J Dent Res 1998;77:589–602, http://dx.doi.org/10.1177/00220345980770041201.
[36] Wu X, Nakagawa M, Teraoka F. Failure morphology of all-ceramic prostheses. Dent Mater J 2012;31:494–8, http://dx.doi.org/10.4012/dmj.2010-167.
[37] Anunmana C, Anusavice KJ, Mecholsky JJ. Interfacial toughness of bilayer dental ceramics based on a short-bar, chevron-notch test. Dent Mater 2010;26:111–7, http://dx.doi.org/10.1016/j.dental.2009.09.003.
[38] Fleming GJP, Nolan L, Harris JJ. The in-vitro clinical failure of all-ceramic crowns and the connector area of fixed partial dentures: the influence of interfacial surface roughness. J Dent 2005;33:405–12, http://dx.doi.org/10.1016/j.jdent.2004.10.025.
[39] Suo Z, Hutchinson JW. Interface crack between two elastic layers. J Fract 1990;43:1–18, http://dx.doi.org/10.1007/bf00018123.
[40] Guazzato M, Albakry M, Ringer SP, Swain MV. Strength, fracture toughness and microstructure of a selection of all-ceramic materials. Part I. Pressable and alumina glass-infiltrated ceramics. Dent Mater 2004;20:441–8, http://dx.doi.org/10.1016/j.dental.2003.05.003.
[41] Guazzato M, Albakry M, Ringer SP, Swain MV. Strength, fracture toughness and microstructure of a selection of all-ceramic materials. Part II. Zirconia-based dental ceramics. Dent Mater 2004;20:449–56, http://dx.doi.org/10.1016/j.dental.2003.05.002.
[42] Benazzi S, Kullmer O, Grosse IR, Weber GW. Using occlusal wear information and finite element analysis to investigate stress distributions in human molars. J Anat 2011;219:259–72, http://dx.doi.org/10.1111/j.1469-7580.2011.01396.x.
[43] Guazzato M, Proos K, Quach L, Swain MV. Strength, reliability and mode of fracture of bilayered porcelain/zirconia (Y-TZP) dental ceramics. Biomaterials 2004;25:5045–52, http://dx.doi.org/10.1016/j.biomaterials.2004.02.036.
[44] Verdonschot N, Fennis WM, Kuijs RH, Stolk J, Kreulen CM, Creugers NH. Generation of 3-D finite element models of restored human teeth using micro-CT techniques. Int J Prosthodont 2001;14:310–5, http://dx.doi.org/10.1016/j.jdent.2005.02.010.